



Evaluation of Magnetic Parameters and Kinetics of the Magnetic Nanoparticles in High Magnetic Fields and its Potential Applications

Mark Christopher Arokiaraj^{1*}, Aleksandr Liubimtcev²

¹Department of Cardiology, Pondicherry Institute of Medical Sciences, Pondicherry, India; ²Quickfield Support Team, Tera Analysis Ltd., Svendborg, Denmark

Abstract

Edited by: Slavica Hristomanova-Mitkovska
Citation: Arokiaraj MC, Liubimtcev A. Evaluation of Magnetic Parameters and Kinetics of the Magnetic Nanoparticles in High Magnetic Fields and its Potential Applications. Open Access Maced J Med Sci. 2020 Feb 15; 8(A):24-36. <https://doi.org/10.3889/oamjms.2020.3256>
Keywords: Magnetic nanoparticles; High magnetic fields; Electromagnetic finite element analysis; Angiogenesis; Tissue engineering; Halbach array
***Correspondence:** Mark Christopher Arokiaraj, Department of Cardiology, Pondicherry Institute of Medical Sciences, Pondicherry, India. E-mail: christomark@gmail.com

Received: 20-Jun-2019
Revised: 14-Nov-2019
Accepted: 05-Feb-2020

Copyright: © 2020 Mark Christopher Arokiaraj, Aleksandr Liubimtcev
Funding: This research did not receive any financial support

Competing Interests: The authors have declared that no competing interests exist

Open Access: This is an open-access article distributed under the terms of the Creative Commons Attribution-NonCommercial 4.0 International License (CC BY-NC 4.0)

BACKGROUND: Multifunctional nanoparticles are known for their wide range of biomedical applications. Controlling the magnetic properties of these nanoparticles is imperative for various applications, including therapeutic angiogenesis.

AIM: The study was performed to evaluate the magnetic properties and their control mechanisms by the external magnetic field.

METHODS: A 100 nm magnetic nanoparticle was placed in the magnetic field, and parametrically, the magnet field strength and distance were evaluated. Various models of magnetic strength and disposition were evaluated. Magnetic flux density, force/weight, and magnetic gradient strength were the parameters evaluated in the electromagnetic computational software.

RESULTS: The seven-coil method with three centrally placed coils as Halbach array, and each coil with a flux density of 7 Tesla, and with a coil dimension of 20 cm × 20 cm (square model) of each coil showed a good magnetic strength and force/weight parameters in a distance of 15 cm from the centrally placed coil. The particles were then evaluated for their motion characteristics in saline. It showed good displacement and acceleration properties. After that, the particles were theoretically assessed in a similar mathematical model after parametrically correcting the drag force. After the application of high drag forces, the particles showed adequate motion characteristics. When the particle size was reduced further, the motion characteristics were preserved even with high drag forces.

CONCLUSION: There is potential for a novel method of controlling multifunctional magnetic nanoparticles using high magnetic fields. Further studies are required to evaluate the motion characteristics of these particles *in vivo* and *in vitro*.

Introduction

Magnetic nanoparticles are multifunctional and they are also carriers of various biomolecules. They are currently used for various biomedical applications [1], [2], [3]. The particle has unique properties after surface modification and conjugation with various biomolecules [4], [5], [6], [7], [8]. Their physical and certain biochemical properties can be magnetically controlled [8]. In the previous studies to a very limited extent, the motion of the particles was studied and the magnetic field strength used was minimal. The purpose of this study was to evaluate the magnetic properties of these magnetic nanoparticles in large magnetic field strength and to identify its magnetic and motion dynamics in saline and tissues. The details of the magnetic properties of these magnetic nanoparticles in large magnetic field are currently not available. The study was performed with the focus of cardiovascular applications, and the results could also be extrapolated to a wide range of applications, for example, neurovascular and renal diseases. The magnetic nanoparticles have shown the potentials of angiogenesis in the previous study [9]. Hence, steering the magnetic nanoparticles in the required areas could

result in angiogenesis, which could evolve as a potential novel therapy. The results would be useful for a wide range of applications in the biomedical fields.

Methods

Their interaction in high magnetic field needs to be studied in detail. Magnetic field and intensity follow the basic principles of magnetism, i.e., Maxwell's and Faraday's equations [10], [11]. In this study, we performed an electromagnetic simulation of magnetic field with high magnetic intensity by parametric variations in intensity position and magnetic nanoparticle sizes. The trend in magnetic field intensity and magnetic field force predominantly in X-axis and in some Y-axis force parameters was computed. The magnetic field strength of each magnetic coil was increased to 7T. Furthermore, to increase the magnetic strength, further the coil dimensions were varied and then the Halbach array technique to amplify magnetic intensity was used [12], [13]. The position and the number of coils

were increased and the angulations were modified and thereafter the results were studied. The standard particle size of 100 nm was assumed in most experiments. The particle dimensions were reduced later parametrically and their magnetic properties were studied.

The force/weight acting on the particle in the various models was also estimated. A 100 nm magnetic nanoparticle was placed in the magnetic field and using finite element analysis, the electromagnetic behavior of the particle was studied in Quickfield software, and the results were computed two-dimensionally, for evaluation, single coils were used. The coil strength was increased by increasing the number of turns in the coils. When the force acting on the particles was evaluated, the displacement and acceleration kinetics of the particles were studied in saline and to model the tissues, the drag forces were increased up to 1000 times to simulate the motion in tissues with higher values. In the initial part of the study, nickel (Ni) rings were placed at various locations from the electromagnets and maximum electric current (A/C or D/C) was passed in these Ni rings. This is to study the electromagnetic distortions and eddy currents which tend to form by the Ni rings when placed near high magnetic fields. The details of the model and the elaborate results are available in the Quickfield website. The supplement website gives elaborate details of the calculations including force, the force/weight values, and motion dynamics of the nanoparticles.

Supplement website file <http://quickfield.com/publications/MarkArokiaraj>

Initially, a single coil was placed (Figure 1a) and the magnetic flux density and gradient in X-axis were measured by the Quickfield electromagnetic software (Figure 1b). Thereafter, the coils were added, and they had a flux density of 5T at different locations at the point of interest. The flux density and force/weight were measured in X-axis (supplement file 3).

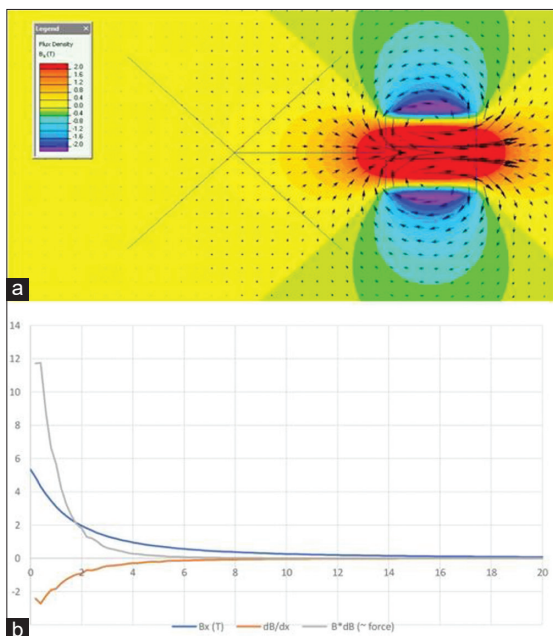


Figure 1a and b: Single coil evaluation in 5T magnetic flux density

Figure 2a shows the placement of the 5T magnets in the +135 and +225, and the polarity of the magnets is the same as that of the magnet placed in the opposite site (0 degree). The zero in Table 2b indicates the surface of the 5T magnet at zero degrees. A high force/weight of about 12 was generated, but it falls acutely after 2cm distance from the magnet. The polarity of the magnets at +135 and -225 degrees was reversed, and the magnet at zero degrees had

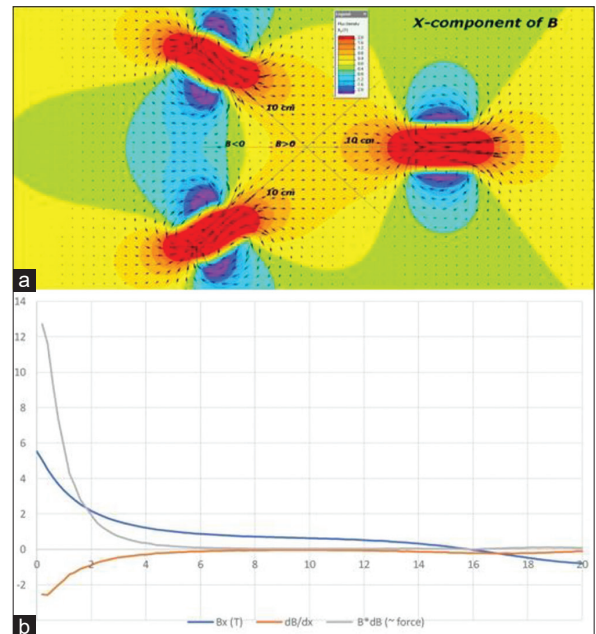


Figure 2a and b: Three 5T coils location (+135 and +225). Force parameters are given in the supplement file 11 (Excel file)

the same polarity, as shown in Figure 3a. The force parameters (Figure3b) were almost the same as the Figure 2 arrangement. Next, the 5T magnets with the

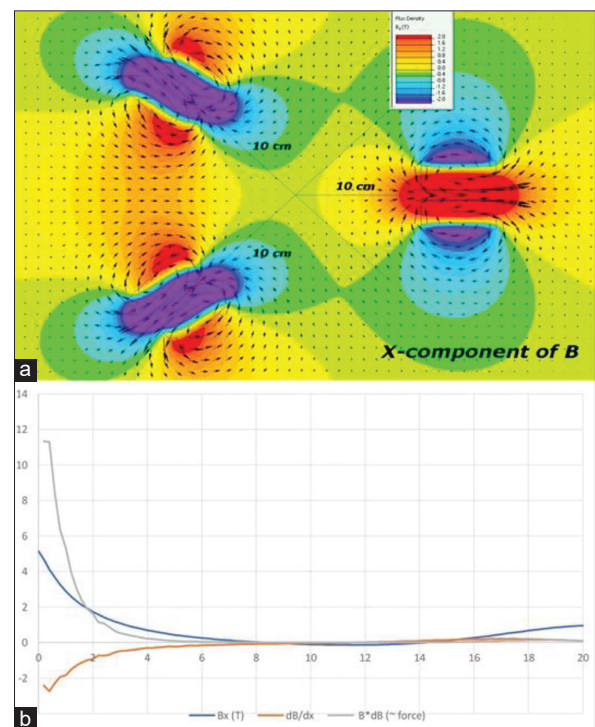


Figure 3a and b: Three 5T coils location (+135 and -225). Force parameters are given in the supplement file 1 (Excel file 1)

same polarity were placed side by side (Figure 4a), and the force parameters showed a high negative force of about 2T (violet areas) in between the 5T magnets. In this arrangement also, the magnetic flux density falls in 2 to 3 cm away from the magnetic field (Figure 4b).

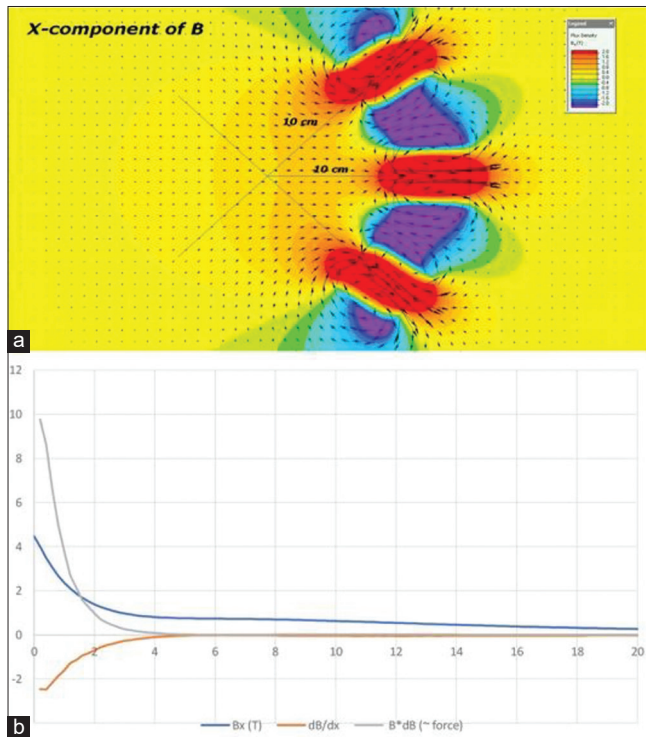


Figure 4a and b: Three 5T coils location (+45 and +315°). Force parameters are given in the supplement file 1 (Excel file 1)

In the next arrangement (Figure 5a) the polarity of the magnets was reversed in the outer magnets. The force parameters showed a fall of the force parameters at 2.5cm to 2T (Figure 5b). In the next arrangement 3 outer 5T coils were placed and 2 coils of 2T was placed

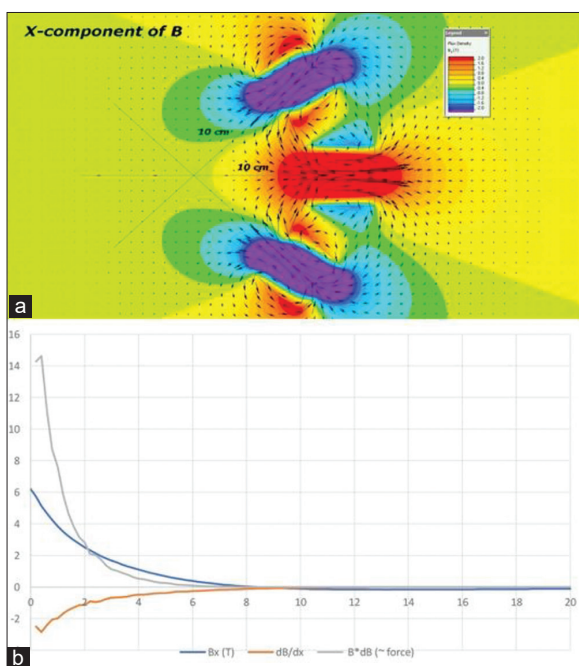


Figure 5a and b: Three 5T coils location (-45 and -315°). Force parameters are given in the supplement file 11 (Excel file)

internally as shown in Figure 6a. The force/weight was high near the magnet and rapidly falls and again at 5–7 cm from the coils, and a spike of increased force/weight was observed (Figure 6b). The force parameters are given in supplement 1e attached 5-coil simulation with 30 cm distance. The analysis in the violet areas

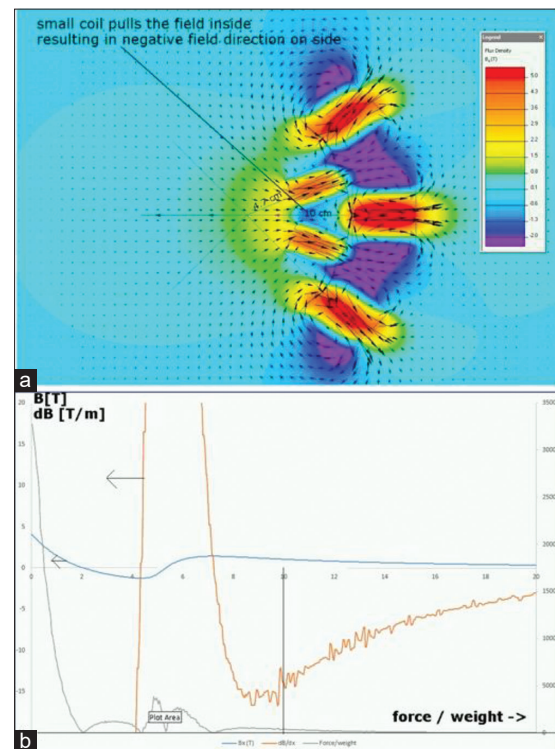


Figure 6a and b: Five-coil simulation force parameters (3 × 5T outer coils and 2 × 2T inner coils located near the point of interest located 10 cm from the central coils)

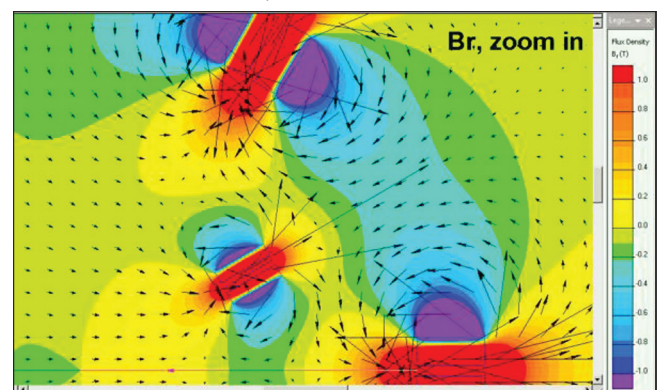


Figure 7a: Five-coil technique with double distance, i.e. the point of interest is located 30 cm from the central coil

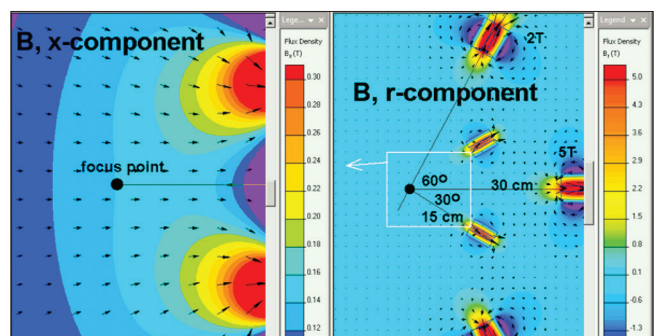


Figure 7b: Five-coil technique with double distance, i.e. the point of interest is located 30 cm from the central coil

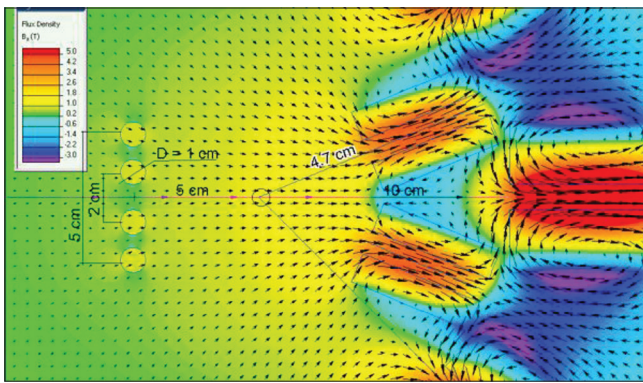


Figure 8a: Simulation with five coils with two Ni rings with A/C current. Force parameters are given in supplement file 2

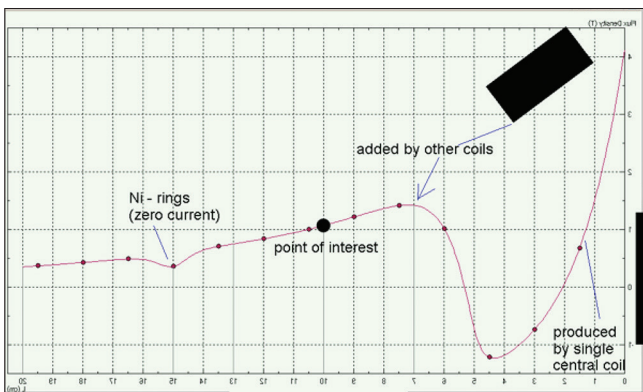


Figure 8b: Simulation with five coils with two Ni rings with A/C current. Force parameters are given in supplement file 2

in Figure 6a is given in supplement file as – violet area evaluation.

The 5T magnets were moved apart, and the point of interest was placed 30cm from the magnetic surface of the magnet set in the x-axis (Figure 7a). The force generated was not appreciable, and it was not significantly different from the closely placed magnets (Figure 7b). However, in between the large magnets, a light blue zone of about 0.8 T was seen (Figure 7b). In the next arrangement the coils were again closely placed, and the point of interest was away from 10cm from the surface of the x-axis magnet (Figure 8a). Ni rings were placed away from the point of interest, and A/C was used in the Ni. However, the magnetic parameters were not significantly different (Figure 8b). In the next arrangement the Halbach array was removed and the 7 magnets with 7T coils were placed serially in C-manner (Figure 9a) and the force parameters were present only near the central magnet. This also emphasizes the importance of Halbach array's contribution to extend the magnetic forces away from the central magnet.

Figure 10a shows the arrangement of coils (seven 7T magnets) with three central coils in the Halbach arrangement. The x-axis magnetic flux density generated after the simulation is shown in Figure 10b, and Figure 10c illustrates the extent of distribution of the flux density from the surface of the central magnet to point 0 located 30cm away from the surface of the central magnet.

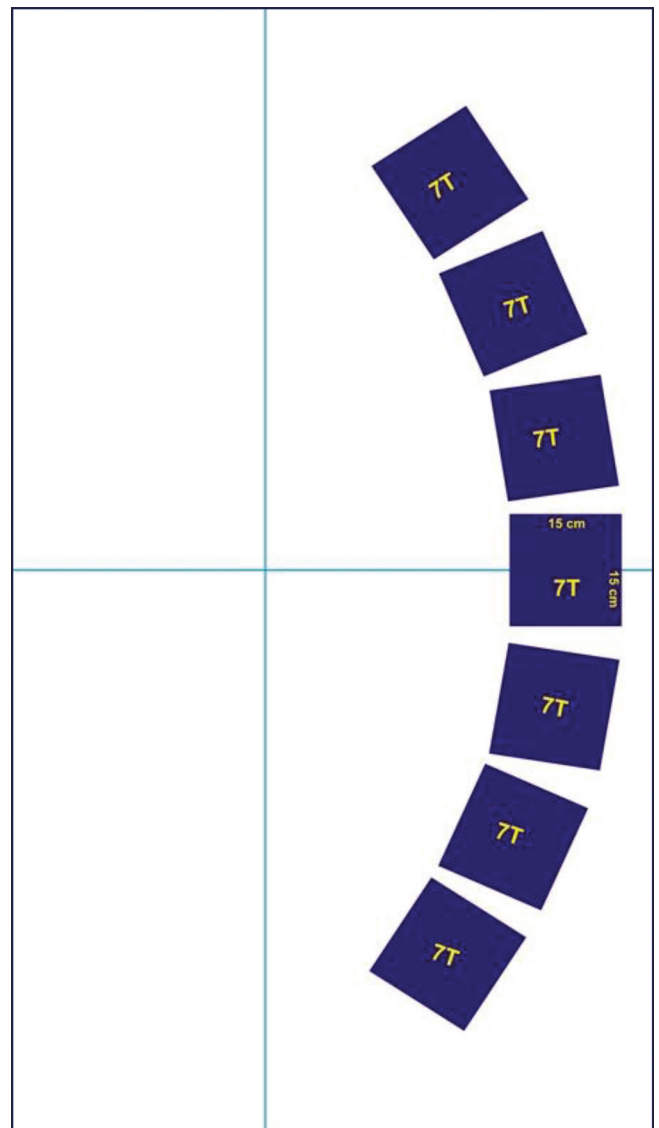


Figure 9a: 7 x 7T coils setup and the point of interest in X-plane

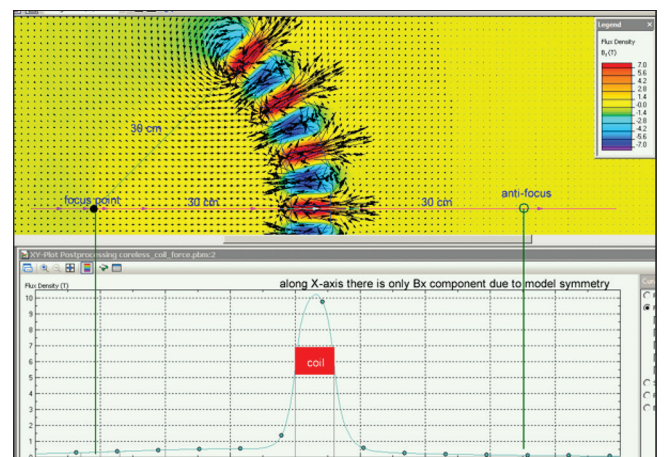


Figure 9b: 7 x 7T coils setup and the point of interest in X-plane

Figure 11 shows the magnetic flux density parameters in a similar seven coil model with three central Halbach. The force parameters in x-axis are given in supplement 28. The force/weight parameters were higher around the magnet, and it extends about 15cm on either

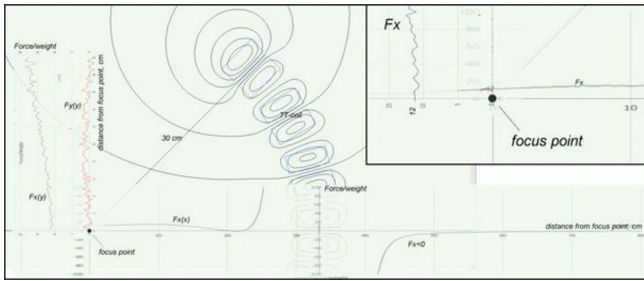


Figure 9c: Results of 7-coil setup with charts showing X and Y forces

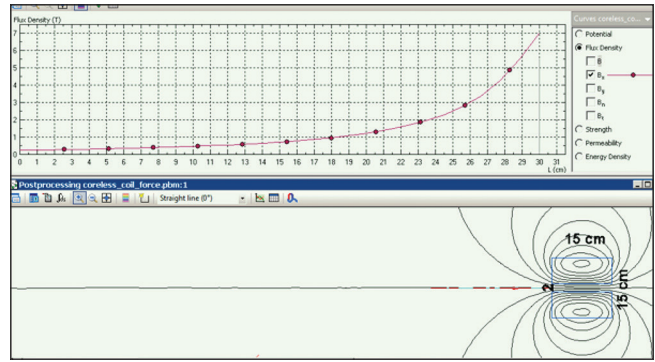


Figure 10c: Seven coils with three coils at central Halbach location – each coil dimension 15 × 15 cm

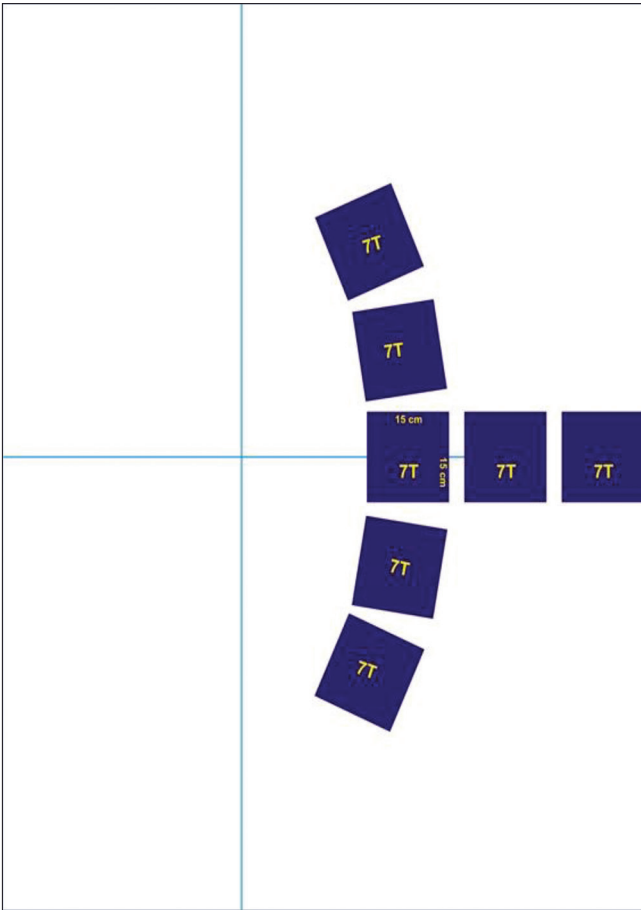


Figure 10a: Seven coils with three coils at central Halbach location – each coil dimension 15 × 15 cm and its flux density. Force parameters are given in supplement file 2

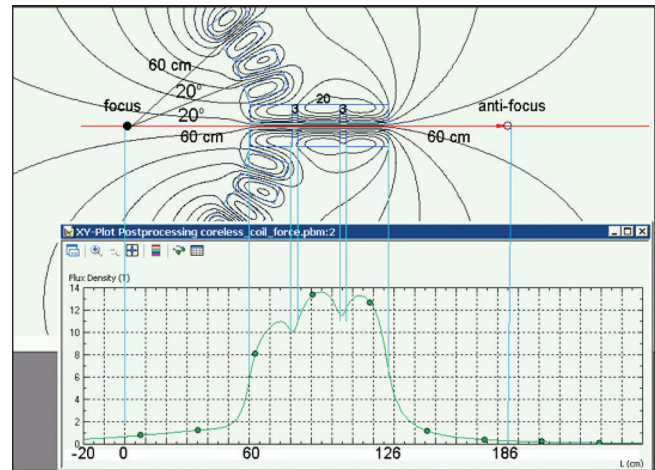


Figure 11: Seven coils with three coils at central Halbach location – each coil dimension 20 × 20 cm. Force parameters are given in supplement 28 (particle size 100 nm)

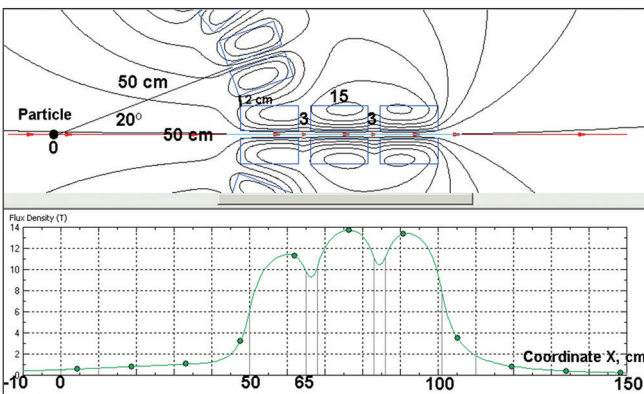


Figure 10b: Seven coils with three coils at central Halbach location – each coil dimension 15 × 15 cm and its flux density. Force parameters are given in supplement file 27

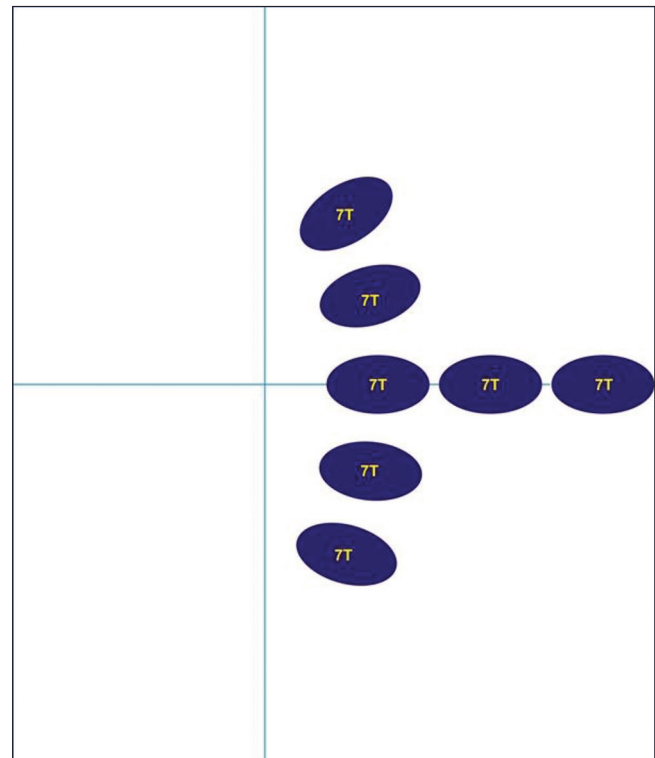


Figure 12a: Ellipsoidal model with seven coils with three central Halbach arrangement (and supplement file 29)

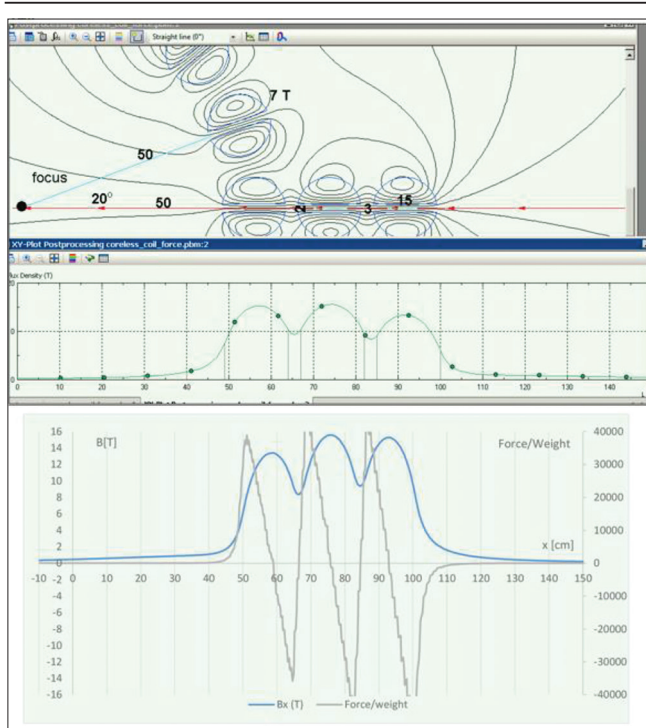


Figure 12b: Ellipsoidal model with seven coils with three central Halbach arrangement. Force parameters are given in supplement file 29

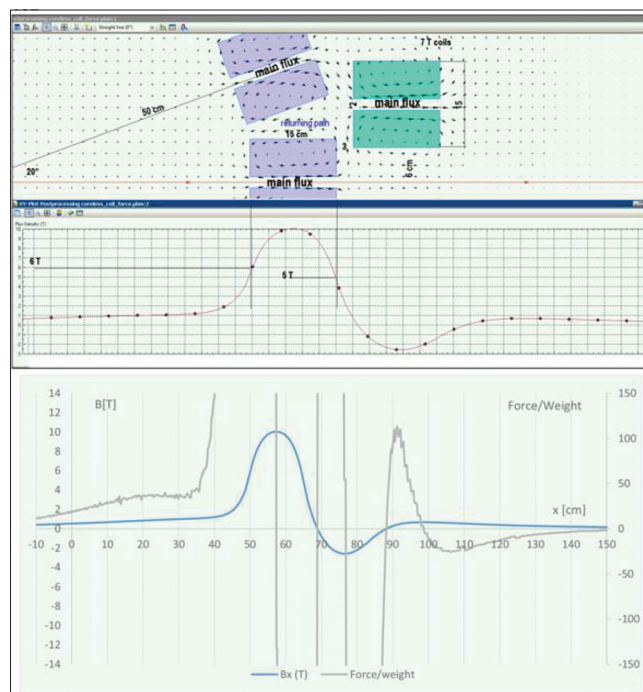


Figure 13b: Back-to-back model with seven coils without three central Halbach arrangement. Force parameters in X-axis are given in supplement file 30

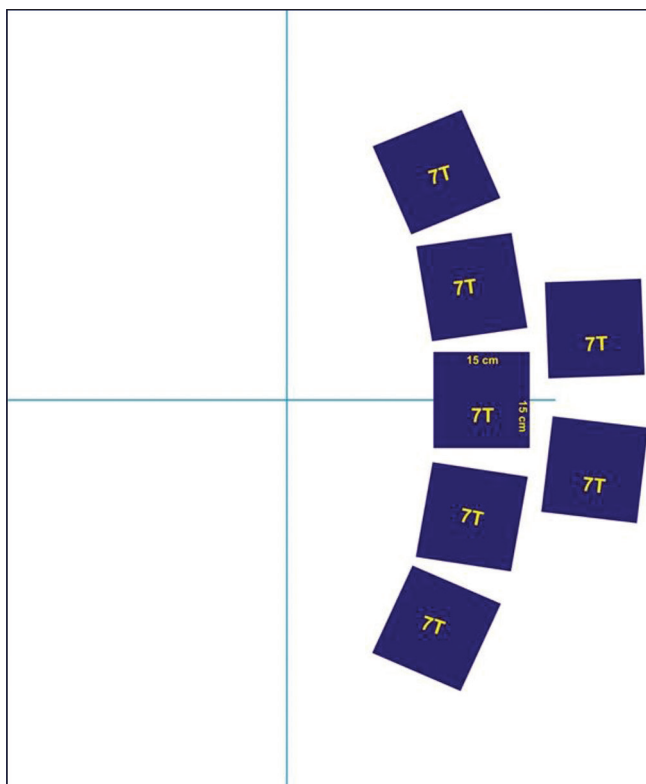


Figure 13a: Model with seven coils without central Halbach arrangement

side of the magnet arrangement. After that, the magnet surface area was altered to elliptical shape (Figure 12a), and the force/ weight parameters and the flux density were not significantly different compared to rectangular models (Figure 12b and c). The x-axis dimension of the ellipsoidal magnets was 15 cm. Subsequently, the study

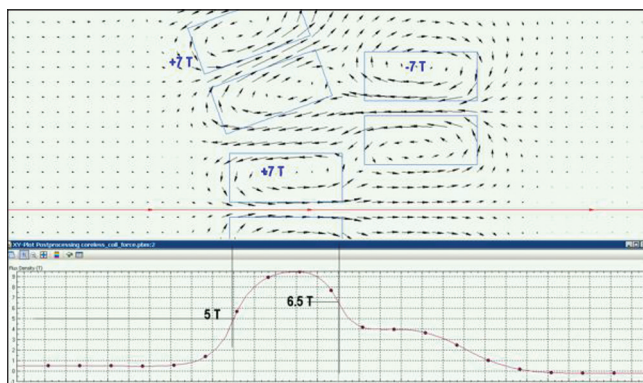


Figure 13c: Results of the back-to-back model with polarity reversed

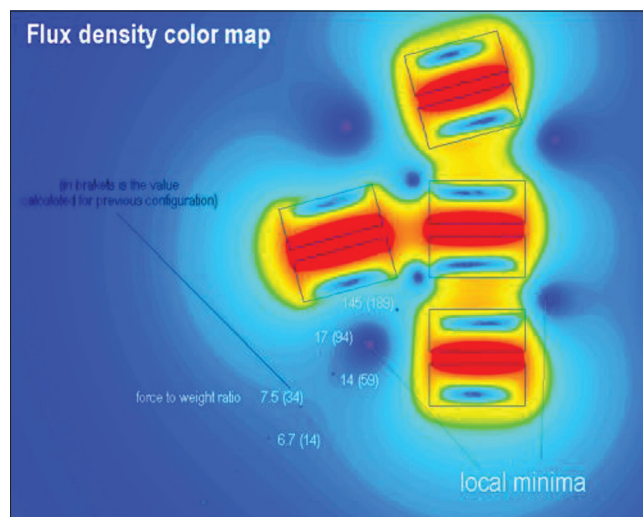


Figure 14: The off-axis (G-model) arrangement of coils and the results – the force/weight values at different locations are seen in the picture (supplement file 35 to 37)

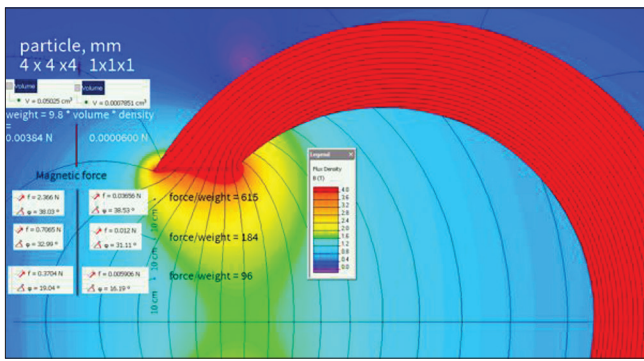


Figure 15a: Horseshoe model evaluation – maximum power achieved due to winding 2.2 T (and supplement file 32 and 33)

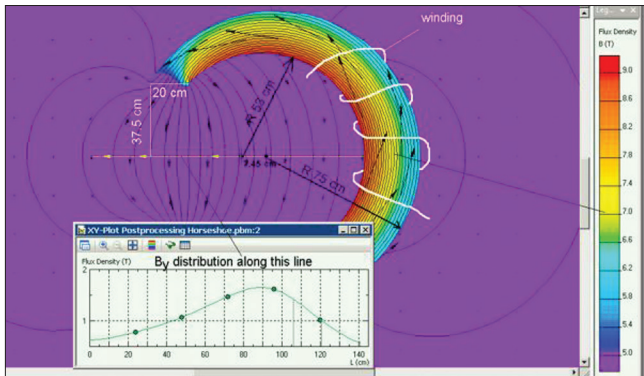


Figure 15b: Horseshoe model evaluation – maximum power achieved due to winding 2.2 T

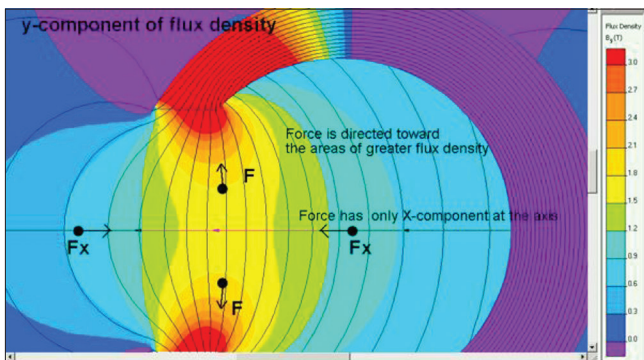


Figure 15c: Horseshoe model evaluation – maximum power achieved due to winding 2.2 T

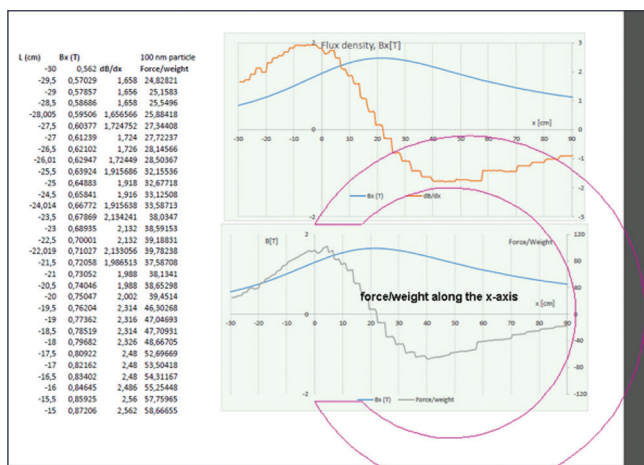


Figure 15d: Horseshoe model evaluation – force/weight distribution values in X- and Y-axis

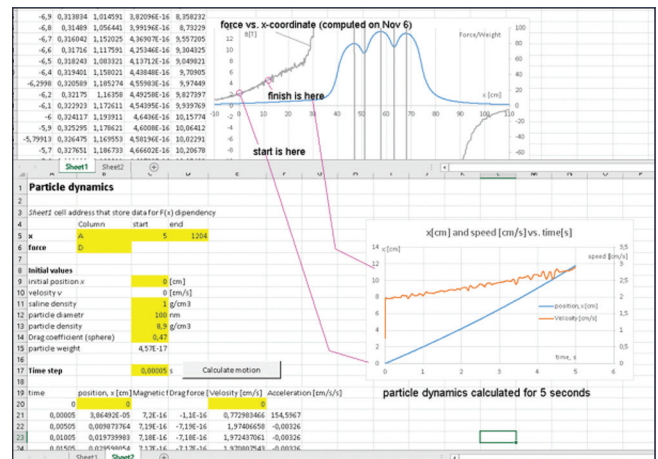


Figure 16a: Magnetic nanoparticle motion dynamics in the magnetic field (supplement file 41, 42)

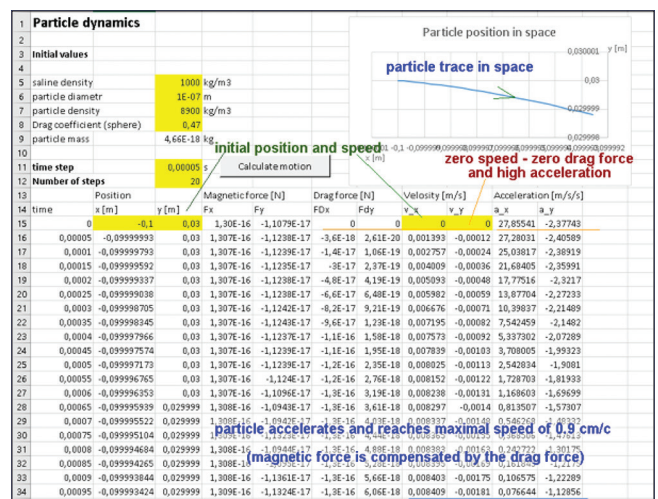


Figure 16b: Calculation of the particle motion in the space/air

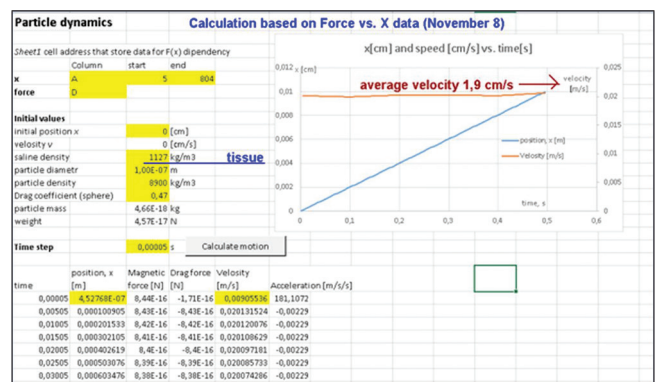


Figure 16c: Calculation of the particle motion in saline with a drag force of 1 (supplement 41)

was performed without the central Halbach arrangement (Figure 13a), and the force/weight parameters were lesser (Figure 13b and c). Then a randomly arranged G model was studied (Figure 14). However, the force/weight and flux density were not appreciable compared to the Halbach arrangement.

The horse-shoe model (Figure 15a) was used to achieve 7T magnetic flux density. However, due

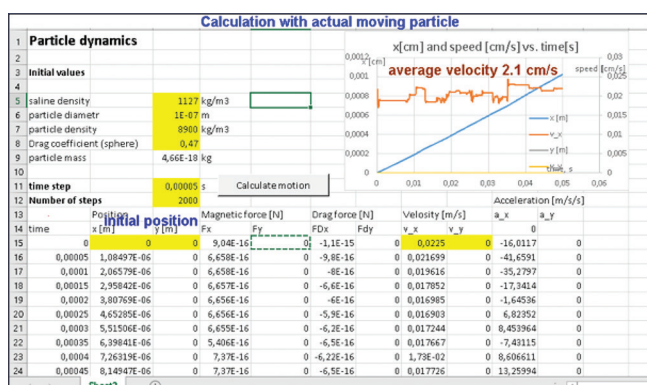


Figure 16d: Particle dynamics with the calculation of actual moving particle in saline (supplement 42, 43)

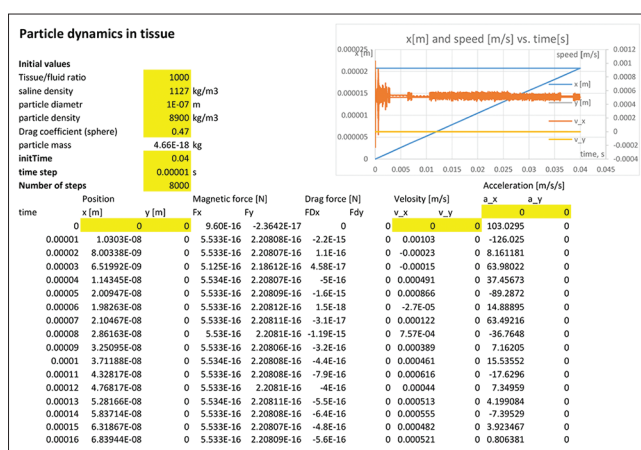


Figure 16g: Particle dynamics with the calculation of actual moving particle in tissue 1000 times more drag force than saline) showing definite displacement with magnetic effect. (supplement 45)

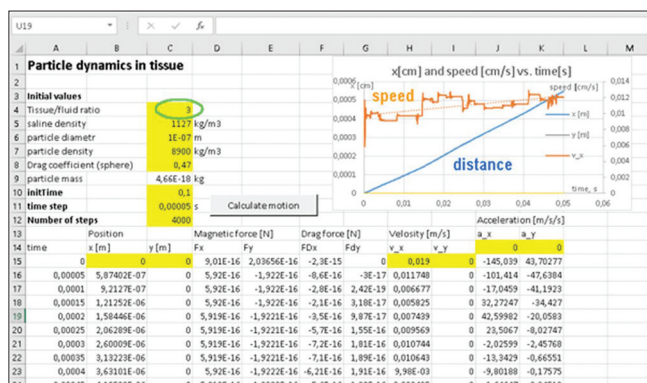


Figure 16e: Particle dynamics with the calculation of actual moving particle in tissue (3 times more drag force than saline) showing definite displacement with magnetic effect (supplement 43)

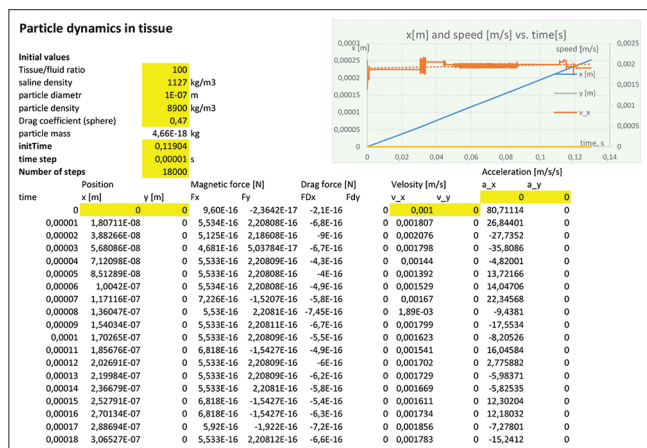


Figure 16f: Particle dynamics with the calculation of actual moving particle in tissue 100 times more drag force than saline) showing definite displacement with magnetic effect (supplement file 45)

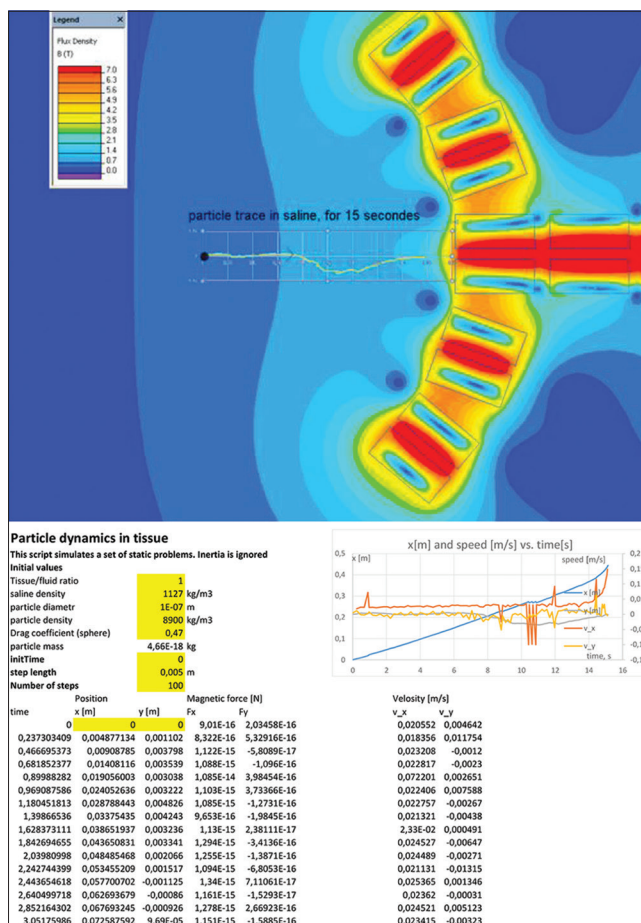


Figure 17: Particle motion dynamics calculation without inertia and a drag force of 1 (supplement 46)

to winding in the coils, only a flux density of 2.2 was obtained. This is due to the phenomenon of magnetic saturation, and to certain extent, this can be improved with Neodymium instead of iron core. The particle was placed in between the horse-shoe, and the force parameters showed dragging the particles on either side of the horseshoe limbs, as shown in the figure 15c. A magnetic flux density of about 2T extends up to 13cm from either side of the horseshoe. (Figure 15b and c). The maximal force/weight was 615.

After that, the particle displacement and acceleration were studied in air/space without resistance or drag force was studied. Figure 16a shows the movement of particles, and the velocity of motion was about 2cm/s. Figure 16b shows the velocity, acceleration, and the magnetic force parameters. Figure 16c shows the motion kinetics of the particles with a minimal drag force of 1. The particles attain a velocity of about 1.9cm/s. Subsequently, the particle dynamics

was studied in saline with a density parameter of saline fixed as 1127kg/m³. The average velocity of the particle was about 2.1cm/s (figure 16d). In the next evaluation to mimic tissues, the saline density was used, and in that a particle drag force three times the normal was simulated Figure 16e. This was primarily to mimic the Vander-wall forces and other intermolecular forces in the tissue. Figure 16f shows the same parameters at a higher drag force of 100 higher than saline. The velocity of particle movement was in the range of 0.2cm/s. Next, with a tissue drag force of 1000 was used. The velocity of particle movement was in the range of 0.02 to 0.06cm/s (Figure 16g).

Figure 17 shows the simulation of the movement of nanoparticles without inertia in saline and a minimal force of 1. The particle trajectory can be seen in figure 1, and the nanoparticle moves towards the magnetic arrangement. This proves that the nanoparticles can be controlled by the magnetic force appreciably, and the particles can move inside the tissues at very high magnetic strength. Figure 18 showed the particle movement towards the magnetic field when the drag force in saline was 1000. The trajectory of the particle motion is seen and the velocity is slower. Finally, the magnetic size of the nanoparticle was reduced from 100nm to 15nm, and with the drag force of 1000, the particle motion was studied. The velocity attained was

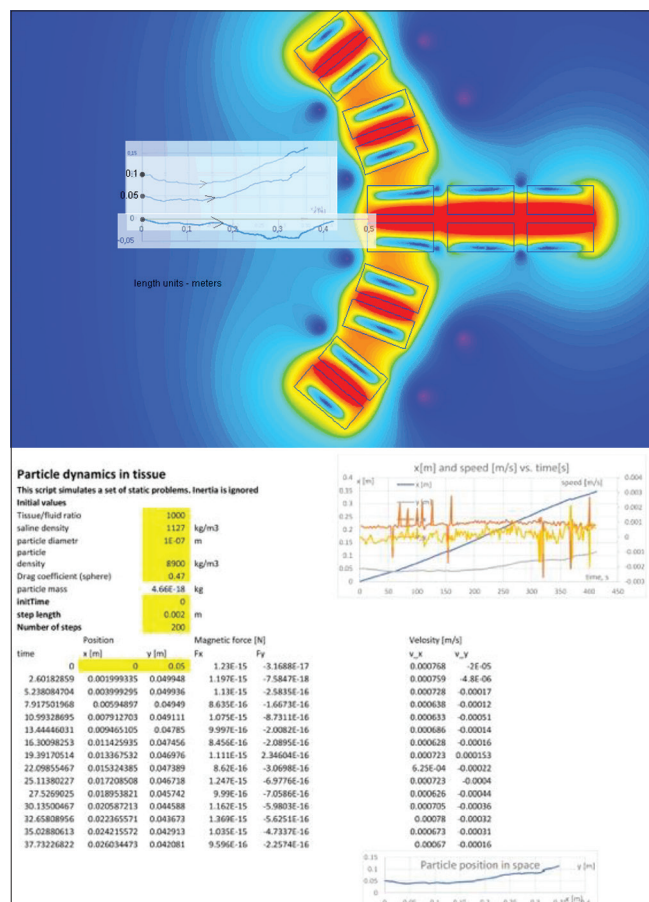


Figure 18: Particle motion dynamics calculation without inertia and a drag force of 1000 and the particle size of 100 nm (supplement 47)

lower than the velocity of 100nm particle, which was 0.02cm/s and in the later, it was about 0.04 to 0.06cm/s (Figure 19).

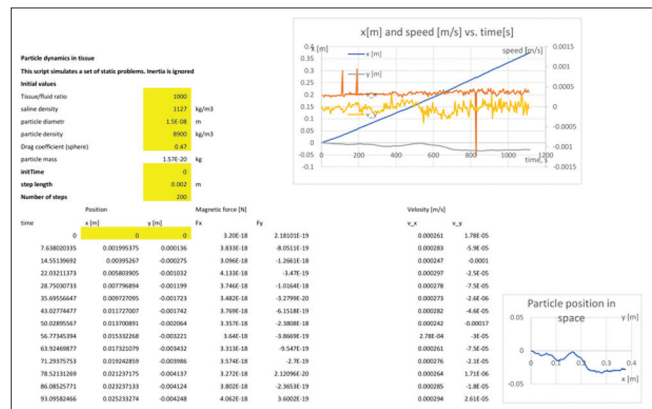


Figure 19: Particle motion dynamics calculation without inertia and a drag force of 1000 and the particle size of 15 nm (supplement 48)

Interestingly in the violet areas of the results (Figure 20) interposed between the magnets, the force on the 100 nm particle would be 0.19e-12 N. This would be approximately 4100 times the particle weight. It will be a tremendous joint, and the particle will accelerate rapidly, reaching the maximal velocity of 0.32 m/s (in saline). Within 50 ms, the particle would hit the side of the coil (the distance to the coil is only 1.5 cm) – the picture attached. The result could be a bit unrealistic because in the model we presume that magnetic field is instantly switched on (or the particle

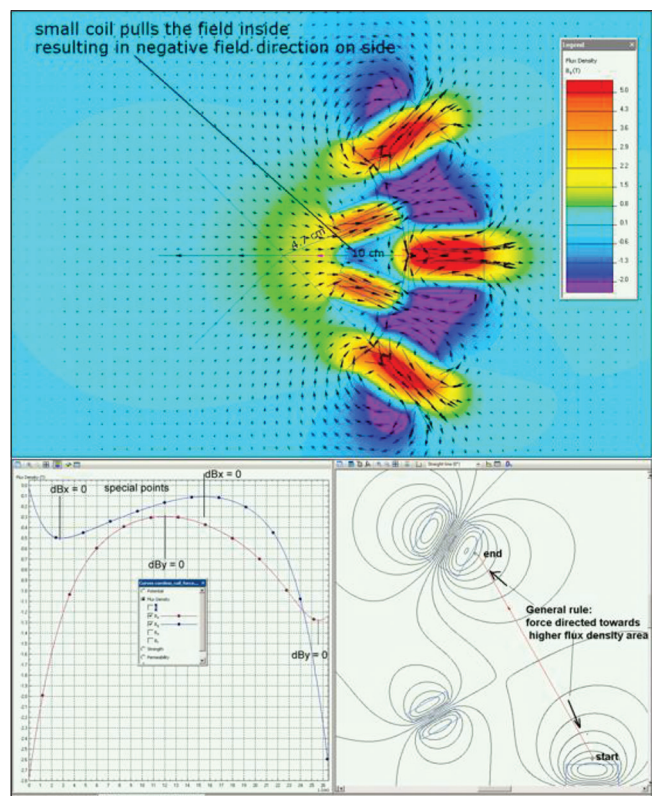


Figure 20: Jacobian line matrix assessment for Y-axis force between two coils in the violet areas in the following model. Force values of the Jacobian line matrix assessment are given in the supplement file (Y-axis Jacobian line matrix assessment) (supplement file 24)

appears suddenly in the already energized magnetic field).

In real life, the particle would travel some distance before reaching the zone of high field intensity. Or else, in case of switching magnetic field, it will take some time to energize the coil fully.

The force/weight parameters on the magnetic nanoparticles reflect the magnetic controllability of the particles. The dB/dx indicates the magnetic flux density, and higher the magnetic flux generated results in more force acting on the particles. The higher the distance the force/weight parameters and the flux density are observed the higher the degree of the distance to which the particles are controlled. The various models tested were developed by changing the shape, dimensions, and the number of the magnetic coils to achieve an optimal magnetic flux density. The magnetic flux density achieved in the Y-axis (dB/dy) is comparatively lesser figure than dB/dx . However, the flux density reached in one axis, i.e. dB/dx , is good enough to regulate the displacement of the magnetic nanoparticles. The best results are achieved by seven numbers of coils with 2 in the central Halbach array. By increasing the surface of the coils from 5 cm to 20 cm, the flux density achieved was higher. However, after reaching the coil size of 20 cm, there was no further increase in the flux density distance or the distance of the force/weight values from the central coil. This could change the angle subtended ($\cos \theta$) by the magnetic coils with respect to neighboring other coils. The Jacobian matrix analysis also revealed similar results for dB/dx and dB/dy (Figure 9c). The ellipsoidal model and the back-to-back placement of coils did not enhance the results; and in fact, the force/wt. and the magnetic flux density parameters were lesser compared to the square models of the coils. The displacement of the particles was demonstrated in saline when the results were tested with increased drag forces. The movement of the particles was higher when the inertia of the particles was ignored. The displacement parameters were evident even when the magnetic nanoparticle size was reduced to 15 nm. Hence, looking at the results, it is possible to achieve good control on the particles by external application of magnetic field within a range of 10–15 cm, and the computational results can be seen in saline and possibly in the tissues also which needs to be evaluated further. Elaborate presentation of the robust data is not possible within the scope of this article. Hence, the details are further seen in the Quickfield reference website with a supplement to this article, which the readers of this study can go through.

Discussion

The study results show the electromagnetic behavior of the magnetic nanoparticles in the magnetic field. The purpose of the study was to increase the force density as well as the magnetic field gradient to maximum

possible higher limits. The maximum distance was 11 cm distance where a force/weight ratio of about 300 at 11 cm length was achieved in the X-axis. This can be used for therapeutic purposes. The magnetic nanoparticles can be injected in the retrosternal space in a line; and the movement of the magnetic nanoparticles can be controlled with external magnetic field to the target arteries which could be left internal mammary artery (LIMA) adjacent to the left anterior descending artery (i.e., LIMA to LAD grafting). The neighboring arteries to the coronaries can also be utilized as a potential target. However, this needs to be evaluated in future experimental studies for further validation and observations. The motion of the magnetic nanoparticles was already demonstrated from the surface, and the motion of the magnetic nanoparticles was studied in detail including the Brownian motion of the surrounding fluid and dipole-dipole interaction of the particles among themselves has some effect on the trajectory, however, this change in the trajectory is minimal [15], [16].

Coronary artery bypass, chronic total occlusions, and peripheral vascular surgery

The conventional coronary artery bypass surgery and peripheral vascular surgery are routinely performed, and they are effective as a therapy. The 1-year mortality rate in coronary artery bypass surgery is about 6.2%. The post-operative neurological complications are seen in about 1.4% [17], acute renal failure in 2%, and nosocomial infections are seen in 10% of patients [18], [19], [20], [21], [22]. Furthermore, the complication rates are more in frail individuals. These surgeries tend to have along waiting period also for various logistic reasons [23]. Hence, a simple novel therapy as a bypass technique would be potentially useful. Peripheral vascular surgeries are associated with a graft occlusion rate of 10%, post-operative infections, and hemorrhages of 5% each and a mortality rate of 3% [24], [25].

Chronic total occlusions have a success rate of about 60–70% and the revascularization benefits are still debatable [26]. A sizable number of patients with coronary artery disease, i.e., 5–10% are classified having refractory angina, and they do not have suitable therapy. In this large subgroup of patients the nanoparticles if they induce angiogenesis, it will be therapeutically very useful [27], [28].

Angiogenesis focus

Angiogenesis can happen when the endothelial cells and extracellular matrix crosstalk and sprouting happens with the effect of VEGF which is a powerful stimulus for angiogenesis. The cross-wiring is further stimulated by hypoxia and certain electrochemical stimuli [29], [30], [31], [32], [33]. However, angiogenesis is complicated due to very short half-life of pro-angiogenic factors and its rapid clearance by the surrounding tissues [29]. The violet areas in the five-coil

simulation (Figures 20 and 21) with a distance of 15 cm between the coils also show high force values in the acceptable range of 15 cm. This potential benefit can be utilized, for example, by interposing a tissue/or an ischemic limb; and the magnetic nanoparticle coated with functional biomolecules can be injected in specific locations for therapeutic purposes to form collaterals. This can induce angiogenesis with VEGF conjugation or it can use for therapeutic occlusion. Furthermore, an internally placed magnet can absorb the magnetic nanoparticles on to the surface.

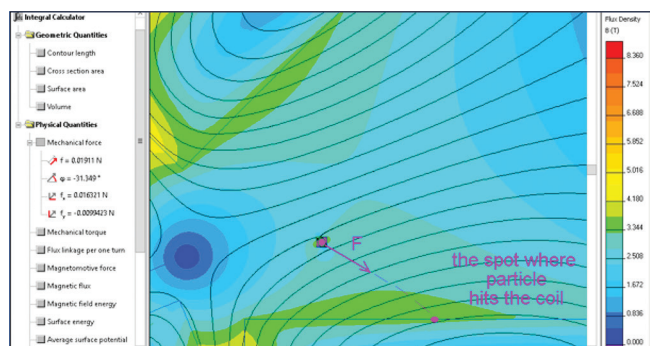


Figure 21: Particle acceleration in the violet areas (supplement file 22 for force values in the violet areas)

Feasibility for percutaneous coronary artery bypass technique

Formation of collaterals between the coronary arteries and adjacent arteries such as the right and LIMA, as well as the epigastric arteries, is theoretically feasible by this technique. The idea is very promising; however, this needs to be evaluated by further studies *in vitro* and *in vivo*. As an extension of this principle, it can be used for collaterals in peripheral and cerebrovascular arteries also. In modern times, robotic cardiac surgery has been developed in advanced centers. However, despite advancements due to high working cost and the large learning curve, the technology is still in the developing stages only [34].

Coagulation focus

The nanoparticles conjugated with pro-coagulation biomolecules and coagulation can be induced at the target locations. This can be used to control or modulate bleeding when required in specific focussed areas for hemostasis. Conversely, anticoagulation can be induced in the necessary locations by appropriate conjugations.

Renal interventions

The glomerulus filters the magnetic nanoparticle of sizes less than 10 nm, and thereby, their applications

could be widened for potential renal therapies. This could be in the scenario of immune complex diseases or toxic clearances. However, this is preliminary and needs to be extensively studied.

Toxicity of magnetic nanoparticles

Magnetic nanoparticles are toxic in higher doses [35]. The toxic dose is in the range of 150–300 mg/kg. At this higher dose, it can cause myocardial necrosis and oxidative damages. Liver and spleen were the significant organs affected at a dosage of 1.7 g Fe/kg.

Velocity and controlled displacement kinetics

The particles had maximal velocity kinetics of 32 cm/s when the particles were placed in air subjected to an external magnetic field. The venous blood has a velocity of 10–15 cm/s [36]. Hence, when the magnets are placed internally, a good acceleration toward the coil can be achieved. In tissues, the particles are encountered with resistance due to the intermolecular resistance forces which prevent the displacement of the particles. The displacement of the particles happens even when the resistance forces or the drag forces were kept 3–5 times that of the saline, as shown in Figure 16e and f. The controlled displacement is enough to prove the control of the particles at least in one axis by external magnetic forces.

Heat generation

High magnetic energy generation would be associated with heat generation, and this needs to be quantified. Since the magnetic field source analyzed in this study is placed externally, the heat generation can be controlled by various cooling methods which can be placed outside.

Limitations and future perspectives

The study was performed in a two-dimensional simulation method. 3D computations would give more information as well as the possible additions of more number of coils in the proposed models. Furthermore, the effect of motion of the coils could not be estimated and these are the limitations. To a certain extent in this study, motion studies were simulated using A/C current instead of D/C. However, in the results, there were no apparent changes in the magnetic intensity of force/weight parameters by changing to A/C. The drag force acting on the particles in motion needs to be quantified by experiments. However, the velocity kinetics shows excellent values and this is faster than the venous flow. Hence, the particles can be

trapped or eliminated from the venous system. More details of the kinetics need to be estimated by other studies and experiments. The particle release and control dynamics of the biomolecules at the tissue level need to be determined [37]. Furthermore, the horseshoe model needs to be evaluated at a higher magnetic force level so that controlling the particles is even easier [38]. Perfluorocarbon nanobubbles have been shown to have efficacy in reducing hypoxic cardiomyocyte injury [39]. Furthermore, the perfluorocarbon nanobubbles could be conjugated with magnetic nanoparticles [40]. Hence, this technique after conjugation can be evaluated by bench studies to identify its potential in myocardial salvage in acute coronary syndromes.

Conclusion

There is potential for a novel method of controlling multifunctional magnetic nanoparticles using high magnetic fields. Further studies are required to evaluate the motion characteristics of these particles *in vivo* and *in vitro*.

Authors' contributions

MCA conceived the idea and method, designed the study, interpreted the results, and wrote the paper. AL performed the mathematical analysis, generated the results, and developed the algorithm for motion kinetics evaluation.

Acknowledgment

Sincere thanks to Vladimir Podnos, Director of marketing and support, Quickfield, Tera Analysis Ltd., Canada.

References

- Tran N, Webster T. Magnetic nanoparticles: Biomedical applications and challenges. *J Mater Chem*. 2010;20:8760.
- Cardoso VF, Francesko A, Ribeiro C, Bañobre-López M, Martins P, Lanceros-Mendez S. Advances in magnetic nanoparticles for biomedical applications. *Adv Healthc Mater*. 2017;7(5):1700845. <https://doi.org/10.1002/adhm.201700845>
- Mohammed L, Gomaa H, Ragab D, Zhu J. Magnetic nanoparticles for environmental and biomedical applications: A review. *Particuology*. 2017;30:1-4. <https://doi.org/10.1016/j.partic.2016.06.001>
- Reddy LH, Arias JL, Nicolas J, Couvreur P. Magnetic nanoparticles: Design and characterization, toxicity and biocompatibility, pharmaceutical and biomedical applications. *Chem Rev*. 2012;112(11):5818-78. <https://doi.org/10.1021/cr300068p>
- Dobson J. Remote control of cellular behaviour with magnetic nanoparticles. *Nat Nanotechnol*. 2008;3(3):139-43. PMID:18654485
- Namiki Y, Namiki T, Yoshida H, Ishii Y, Tsubota A, Koido S, *et al*. A novel magnetic crystal-lipid nanostructure for magnetically guided *in vivo* gene delivery. *Nat Nanotechnol*. 2009;4(9):598-606. <https://doi.org/10.1038/nnano.2009.202>
- Mannix RJ, Kumar S, Cassiola F, Montoya-Zavala M, Feinstein E, Prentiss M, *et al*. Nanomagnetic actuation of receptor-mediated signal transduction. *Nat Nanotechnol*. 2008;3(1):36-40. <https://doi.org/10.1038/nnano.2007.418>
- Fu A, Wilson RJ, Smith BR, Mullenix J, Earhart C, Akin D, *et al*. Fluorescent magnetic nanoparticles for magnetically enhanced cancer imaging and targeting in living subjects. *ACS Nano*. 2012;6(8):6862-9. <https://doi.org/10.1021/nn301670a>
- Arokiaraj MC. A novel targeted angiogenesis technique using VEGF conjugated magnetic nanoparticles and *in-vitro* endothelial barrier crossing. *BMC Cardiovasc Disord*. 2017;17(1):209. <https://doi.org/10.1186/s12872-017-0643-x>
- Chikazumi S, Graham CD. *Physics of Ferromagnetism*. 2nd ed. Oxford: Oxford University Press; 1997. p. 118.
- David JJ. *Classical Electrodynamics*. 2nd ed. New York: Wiley; 1975.
- Halbach K. Applications of permanent magnets in accelerators and electron storage rings. *J Appl Phys*. 1985;57:3605-8.
- Sarwar A, Nemirovski A, Shapiro B. Optimal Halbach permanent magnet designs for maximally pulling and pushing nanoparticles. *J Magn Magn Mater*. 2012;324(5):742-54. <https://doi.org/10.1016/j.jmmm.2011.09.008>
- Elliott R. Transformers-the Basics. In: *Beginner's Guide to Transformers*. Elliott Sound Products; 2010. <https://sound-au.com/xfrmr.htm>. Retrieved 2011-03-17.
- Kulkarni S, Ramaswamy B, Horton E, Gangapuram S, Nacev A, Depireux D, *et al*. Quantifying the motion of magnetic particles in excised tissue: Effect of particle properties and applied magnetic field. *J Magn Magn Mater*. 2015;393:243-52. <https://doi.org/10.1016/j.jmmm.2015.05.069>
- Schaller V, Kräling U, Rusu C, Petersson K, Wipenmyr J, Krozer A, *et al*. Motion of nanometer sized magnetic particles in a magnetic field gradient. *J Appl Phys*. 2008;104:93918. <https://doi.org/10.1063/1.3009686>
- Vanninen R, Aikiä M, Könönen M, Partanen K, Tulla H, Hartikainen P, *et al*. Subclinical cerebral complications after coronary artery bypass grafting: Prospective analysis with magnetic resonance imaging, quantitative electroencephalography, and neuropsychological assessment. *Arch Neurol*. 1998;55(5):618-27. <https://doi.org/10.1001/archneur.55.5.618>
- Khorsandi M, Shaikhrezai K, Zamvar V. Complications of

- coronary artery bypass grafting surgery. *Pan Vasc Med.* 2015;:2359-67. https://doi.org/10.1007/978-3-642-37078-6_233
19. Diodato M, Chedrawy EG. Coronary artery bypass graft surgery: The past, present, and future of myocardial revascularisation. *Surg Res Pract.* 2014;2014:726158. <https://doi.org/10.1155/2014/726158>
PMid:25374960
 20. Glance LG, Osler TM, Mukamel DB, Dick AW. Effect of complications on mortality after coronary artery bypass grafting surgery: Evidence from New York state. *J Thorac Cardiovasc Surg.* 2007;134(1):53-8. <https://doi.org/10.1016/j.jtcvs.2007.02.037>
PMid:17599486
 21. Moazzami K, Dolmatova E, Maher J, Gerula C, Sambol J, Klapholz M, *et al.* In-hospital outcomes and complications of coronary artery bypass grafting in the United States between 2008 and 2012. *J Cardiothorac Vasc Anesth.* 2017;31(1):19-25. <https://doi.org/10.1053/j.jvca.2016.08.008>
PMid:27887898
 22. Safaie N, Montazerghaem H, Jodati A, Maghamipour N. In-hospital complications of coronary artery bypass graft surgery in patients older than 70 years. *J Cardiovasc Thorac Res.* 2015;7(2):60-2. <https://doi.org/10.15171/jcvtr.2015.13>
PMid:26191393
 23. Cesena FH, Favarato D, César LA, de Oliveira SA, da Luz PL. Cardiac complications during waiting for elective coronary artery bypass graft surgery: Incidence, temporal distribution and predictive factors. *Eur J Cardiothorac Surg.* 2004;25(2):196-202. <https://doi.org/10.1016/j.ejcts.2003.11.004>
PMid:14747112
 24. Schepers A, Klinkert P, Vrancken Peeters MP, Breslau PJ. Complication registration in patients after peripheral arterial bypass surgery. *Ann Vasc Surg.* 2003;17:198-202. <https://doi.org/10.1007/s10016-001-0290-6>
PMid:12616358
 25. Slovut DP, Lipsitz EC. Surgical technique and peripheral artery disease. *Circulation.* 2012;126:1127-38. <https://doi.org/10.1161/circulationaha.111.059048>
PMid:22927475
 26. Sianos G, Konstantinidis NV, Di Mario C, Karvounis H. Theory and practical based approach to chronic total occlusions. *BMC Cardiovasc Disord.* 2016;16:33. <https://doi.org/10.1186/s12872-016-0209-3>
PMid:26860695
 27. Mukherjee D. Management of refractory angina in the contemporary era. *Eur Heart J.* 2013;34:2655-7.
PMid:23739242
 28. Henry TD, Satran D, Jolicoeur EM. Treatment of refractory angina in patients not suitable for revascularization. *Nat Rev Cardiol.* 2014;11(2):78-95. <https://doi.org/10.1038/nrcardio.2013.200>
PMid:24366073
 29. Gorski T, De Bock K. Metabolic regulation of exercise-induced angiogenesis. *Vasc Biol.* 2019;1:H1-8.
 30. Cappelletto A, Zacchigna S. Cardiac revascularization: State of the art and perspectives. *Vasc Biol.* 2019;1:R1-5.
 31. Carmeliet P. Mechanisms of angiogenesis and arteriogenesis. *Nat Med.* 2000;6(4):389-95.
PMid:10742145
 32. Giacca M, Zacchigna S. Virus-mediated gene delivery for human gene therapy. *J Control Release.* 2012;161(2):377-88. <https://doi.org/10.1016/j.jconrel.2012.04.008>
PMid:22516095
 33. Tafuro S, Ayuso E, Zacchigna S, Zentilin L, Moimas S, Dore F, *et al.* Inducible adeno-associated virus vectors promote functional angiogenesis in adult organisms via regulated vascular endothelial growth factor expression. *Cardiovasc Res.* 2009;83(4):663-71. <https://doi.org/10.1093/cvr/cvp152>
PMid:19443424
 34. Pettinari M, Navarra E, Noirhomme P, Gutermann H. The state of robotic cardiac surgery in Europe. *Ann Cardiothorac Surg.* 2017;6(1):1-8. <https://doi.org/10.21037/acs.2017.01.02>
PMid:28203535
 35. Jiang Z, Shan K, Song J, Liu J, Rajendran S, Pugazhendhi A, *et al.* Toxic effects of magnetic nanoparticles on normal cells and organs. *Life Sci.* 2019;220:156-61. <https://doi.org/10.1016/j.lfs.2019.01.056>
PMid:30716338
 36. Coffman JD, Lempert JA. Venous flow velocity, venous volume and arterial blood flow. *Circulation.* 1975;52:141-5. <https://doi.org/10.1161/01.cir.52.1.141>
PMid:1132117
 37. Landry JP, Ke Y, Yu GL, Zhu XD. Measuring affinity constants of 1450 monoclonal antibodies to peptide targets with a microarray-based label-free assay platform. *J Immunol Methods.* 2015;417:86-96. <https://doi.org/10.1016/j.jim.2014.12.011>
PMid:25536073
 38. Arokiaraj MC. Extracorporeal application of eddy brakes to control the magnetic nanoparticles and modulating the drift and diffusion characteristics of these particles in the heart a theoretical assessment. *New Biotechnol.* 2018;44:S8-9. <https://doi.org/10.1016/j.nbt.2018.05.182>
 39. Arokiaraj MC, Menesson E, Cereijo U, Perera S, Mas JM. A novel method to reduce hypoxic myocyte injury. *Cardiol Belarus.* 2019;11:316-30.
 40. Arokiaraj MC. Novel synthesis of magnetic nanoparticles conjugation with perfluorocarbon nanobubbles for potential adjunct therapy of acute myocardial ischaemia. *Folia Cardiol.* 2019;14:425-7.

Supplement file

Supplement website file <http://quickfield.com/publications/MarkArokiaraj>